



^{18}F -sodium fluoride PET/MRI myocardial imaging in patients with suspected cardiac amyloidosis

Mukedaisi Abulizi, MD,^{a,b} Islem Sifaoui, MD,^{a,b} Mijiti Wuliya-Gariepy, MD,^{a,c} Mounira Kharoubi, MD,^{b,c} Jean-Marc Israël, MD,^a Berivan Emsen, MD,^a Diane Bodez, MD,^{b,c} Aurélien Monnet, MSc,^d David Didierlaurent, PhD,^d Vania Tacher, MD,^{a,b} Alain Luciani, MD, PhD,^a Thibaud Damy, MD, PhD,^{b,c} Jean-François Deux, MD, PhD,^{a,b} and Emmanuel Itti, MD, PhD^{a,b}

^a SyMPTOm PET/MRI platform, Departments of Nuclear Medicine and Radiology, CHU Henri Mondor Hospital, AP-HP/U-PEC, Créteil, France

^b Amyloid Research Institute, IMRB U955, U-PEC, Créteil, France

^c Department of Cardiology, CHU Henri Mondor, AP-HP/U-PEC, Créteil, France

^d Siemens Healthineers, Erlangen, Germany

Received Jun 17, 2019; accepted Jul 31, 2019

doi:10.1007/s12350-019-01885-8

Background. We evaluated the diagnostic performance of ^{18}F -NaF PET/MRI in patients with suspected cardiac amyloidosis (CA).

Methods. Twenty-seven consecutive patients underwent myocardial PET 1 hour after injection of 4 MBq/kg ^{18}F -NaF with simultaneous MRI including cine-MRI, T1 and T2 mapping, first-pass and late gadolinium enhancement (LGE). ^{18}F -NaF uptake was measured visually and semi-quantitatively by calculating myocardium-to-blood pool (M/B) ratios. CA was confirmed histologically.

Results. Transthyretin (TTR)-CA was diagnosed in 16 patients, light-chain (AL)-CA in 7, and no-CA in 4. Visual interpretation of ^{18}F -NaF images revealed a relative increase in myocardial uptake in only 3 patients, all with TTR CA, and a relative decrease in 13, including 7 AL CA, 3 no-CA, and 3 TTR CA. M/B ratios were significantly higher in TTR CA (1.00 ± 0.12) than in AL CA (0.81 ± 0.06 , $P = 0.001$) or in no-CA (0.73 ± 0.16 , $P = 0.006$). The optimal M/B cut-off to distinguish TTR CA from AL CA was ≥ 0.90 (Fischer, $P = 0.0005$). By comparison, classification of patients using $^{99\text{m}}\text{Tc}$ -HMDP heart-to-mediastinum ratios with the previously published cut-off ≥ 1.21 reached higher significance ($P < 0.0001$). Among MRI parameters, myocardial T1, LGE score, and extracellular volume were higher in CA than in no-CA patients, 1409 ± 76 vs 1278 ± 35 ms ($P = 0.004$), 10.35 ± 5.30 vs 3.50 ± 3.42 ($P = 0.03$), and 46 ± 10 vs 33 ± 8 % ($P = 0.01$), respectively.

Conclusion. ^{18}F -NaF PET/MRI shows good diagnostic performance when semi-quantification is used. However, contrast is low and visual interpretation may be challenging in routine. PET/MRI could constitute a one-stop-shop evaluation of amyloid load and cardiac function in patients needing rapid work-up. (J Nucl Cardiol 2021;28:1586–95.)

Key Words: Cardiac amyloidosis • ^{18}F -sodium fluoride • myocardial uptake • PET/MRI

Electronic supplementary material The online version of this article (<https://doi.org/10.1007/s12350-019-01885-8>) contains supplementary material, which is available to authorized users.

The authors of this article have provided a PowerPoint file, available for download at SpringerLink, which summarises the contents of the paper and is free for re-use at meetings and presentations. Search for the article DOI on SpringerLink.com.

Reprint requests: Emmanuel Itti, MD, PhD, SyMPTOm PET/MRI platform, Departments of Nuclear Medicine and Radiology, CHU Henri Mondor Hospital, AP-HP/U-PEC, 51 Ave. du Mal de Lattre de Tassigny, 94010 Créteil, France; emmanuel.itti@aphp.fr
1071-3581/\$34.00

Copyright © 2019 American Society of Nuclear Cardiology.

Abbreviations

¹⁸ F-NaF	¹⁸ F-sodium fluoride
PET/MRI	Positron emission tomography/ magnetic resonance imaging
TTR	Transthyretin
AL	Light-chain
CA	Cardiac amyloidosis
^{99m} Tc-	^{99m} Tc-hydroxymethylene
HMDP	diphosphonate
SUV	Standardized uptake value
LGE	Late gadolinium enhancement
NTproBNP	N-terminal pro-brain natriuretic peptide
ROC	Receiver operating characteristics

INTRODUCTION

Amyloidosis is a set of diseases due to the deposition of insoluble fibril within the extracellular matrix of tissues and organs. To date, more than thirty-six responsible proteins are identified, but the most common types of amyloidosis are due to deposition of transthyretin (TTR) or light chains of immunoglobulins (AL).¹ The diagnosis is histological, based on the identification of amyloid deposits by microscopy, with common features: a Congo Red stain, as well as a birefringence in polarized light.² The prognosis is correlated with myocardial and renal involvements.

Transthyretin-related cardiac amyloidosis (TTR CA) is a systemic disease in which mutant (m-TTR) and/or wild-type (wt-TTR) proteins assemble into the myocardial interstitium. More than 100 different amyloidogenic mutations in the TTR gene have been described, and each is associated with clear multisystem involvement, including life-threatening heart failure. Endomyocardial biopsy (EMB) remains the gold standard for definitive diagnosis of TTR CA. Once amyloid deposits are found, additional testing with immunohistochemistry and/or sequence analysis by mass spectroscopy can identify the precursor protein. EMB may be difficult to perform in elderly patients as complications such as arrhythmia, perforation with pericardial effusion, accidental arterial puncture, and pneumothorax may occur in approximately 6% of patients.³

Imaging techniques may progressively surrogate EMB.⁴ MRI is useful to evaluate ventricular function, wall thickening, and myocardial perfusion.⁵ Myocardial scintigraphy using ^{99m}Tc labeled diphosphonates have demonstrated excellent diagnostic performance to identify TTR accumulation in the myocardium.⁶ Recently,

Van Der Gucht et al. showed the first case report of potential diagnostic and technical values of ¹⁸F-sodium fluoride (¹⁸F-NaF) PET/CT in CA.⁷ Indeed, ¹⁸F-NaF PET/CT was able to differentiate TTR CA from AL CA, and was suggested to be more efficient as it demonstrates faster kinetics and then faster imaging time compared to conventional ^{99m}Tc-diphosphonates imaging. These preliminary data were later confirmed in a series of 5 TTR CA and 2 AL CA patients.⁸

Recent developments of hybrid PET/MRI systems make possible to evaluate simultaneously myocardial metabolism and ventricular function within a single exam. In a pilot study including 4 TTR CA and 3 AL CA patients, Trivieri et al. demonstrated this proof of concept.⁹ Therefore, we sought to evaluate the diagnostic performance of ¹⁸F-NaF PET/MRI in a larger cohort of patients with suspected CA, using visual and semi-quantitative image analysis.

MATERIALS AND METHODS

Study Population

Between June 2017 and November 2018, 27 consecutive patients referred to our reference center (GRC Amyloid Research Institute) with strong clinical suspicion of CA underwent ¹⁸F-NaF PET/MRI imaging. Mean age was 70 ± 10 years and 19 were male. Patients with contra-indications for MRI were not included. All had a glomerular filtration rate ≥ 30 mL/min/1.73 m² compatible with contrast agent injection. Data collection was approved by the Direction Interrégionale de la Recherche Clinique Ile-de-France (DC 2009-930) and by our local institutional review board, and all patients gave informed written consent.

PET/MRI Imaging

Simultaneous acquisition of chest ¹⁸F-NaF PET and cardiac MRI was performed on a Biograph mMR 3T scanner (Siemens Healthcare, Erlangen, Germany), starting 1 hour after injection of 4 MBq/kg of ¹⁸F-NaF. Emission images were recorded during 60 minutes on a single 26-cm height thoracic step, without gating. MRI sequences included (1) a T1 Dixon sequence during mid-exhalation breath-hold for attenuation correction purposes; (2) an unenhanced cine steady-state free-precession (SSFP) sequence, acquired in the long-axis 2/3/4-chamber view, followed by a short-axis view encompassing the left ventricle (LV), with retrospective 25-phase ECG gating for LV kinetics measurements; (3) a T1 mapping before and 15 minutes after 0.2 mmol/kg gadolinium injection (Dotarem, Guerbet, Aulnay-sous-Bois, France) in the short and long axes, within a single breath-hold, using the modified look-locker inversion recovery (MOLLI) sequence for tissue characterisation (fibrosis and amyloid load); (4) a T2 mapping using a prototype balanced SSFP sequence with an adiabatic T2

Table 1. MRI acquisition parameters (Biograph mMR scanner)

	Cine SSFP	T1 map	T2 map	Cine SSFP	LGE	PSIR	T1 map
Acquisition plane	Short axis, 4 chambers	Short axis, 4 chambers	Short axis, 2 & 4 chambers	Short axis, 2 & 4 chambers	Short axis, 2 & 4 chambers	Short axis, 4 chambers	Short axis
Repetition time (ms)	52.95	1.06	1.12	52.95	3.9	835	1.06
Echo time (ms)	1.59	2.5	2.6	1.59	1.4	3.3	2.5
Slice thickness (mm)	8	8	6	8	6	8	8
Slice number	20	8	8	20	18	18	8
Flip angle (°)	82	35	35	82	10	10	35
Matrix size	192 × 192	192 × 154	192 × 154	192 × 192	192 × 192	256 × 156	192 × 154
Field of view (mm ²)	300 × 270	340 × 274	340 × 274	300 × 270	300 × 270	300 × 270	340 × 274
Voxel size (mm ²)	1.48 × 1.48	2.13 × 1.41	2.13 × 1.41	1.48 × 1.48	1.48 × 1.98	1.55 × 1.24	2.13 × 1.41
Injection	No injection			Gadolinium injection			

preparation, and acquired at the same conditions than T1 maps, for tissue characterization (edema);¹⁰ (5) a dedicated inversion recovery time scouting sequence to adjust the optimal time of inversion; and (6) late gadolinium enhancement (LGE) images covering the LV in the short and long axes were obtained 10 minutes after gadolinium injection using a segmented 3D inversion recovery gradient-echo T1-weighted sequence and followed by phase-sensitive inversion recovery (PSIR) images, because of suboptimal nulling of the myocardial signal may be encountered in CA.¹¹ Detailed MRI acquisition parameters are summarized in Table 1.

PET Image Analysis

Emission images were reconstructed using an iterative 3D ordered subset expectation maximization algorithm with attenuation correction and point-spread function correction. Myocardial ¹⁸F-NaF uptake was measured by consensus of two nuclear physicians (MA & EI), qualitatively (presence or absence of myocardial ¹⁸F-NaF uptake), and semi-quantitatively by drawing a 2-dimensional anatomical region-of-interest (ROI) encompassing the left myocardium on the 4-cavity MRI image. Another ROI was drawn inside the left ventricle to allow calculation of the myocardium-to-blood pool (M/B) ratio (Figures 1 and 2). Additionally, a basal-to-apical ratio was calculated by drawing a circular ROI over a basal segment and the apex.

HMDP Image Analysis

Early-phase ^{99m}Tc-HMDP scintigraphy was also performed in 24 patients. On the planar thoracic projection, a squared ROI was drawn over the heart and another over the mediastinum, and heart-to-mediastinum (H/M) ratios were calculated, as previously described.¹²

MRI Image Analysis

MRI images were interpreted by consensus of two experienced radiologists (JFD & IS), blinded to clinical data, on a dedicated syngo.via platform (Siemens Healthcare, Erlangen, Germany). Left ventricular ejection fraction (LVEF), indexed end-diastolic volume (EDV), indexed end-systolic volume (ESV), and indexed myocardial mass were calculated on the cine short-axis images using a dedicated software (cvi42, Circle Cardiovascular Imaging Inc, Calgary, Canada). Maximal septal thickening was measured on the end-diastolic short-axis cine image acquired at the middle part of the left ventricle, T1 and T2 maps were obtained after applying a fast variational non-rigid registration algorithm to correct for residual cardiac and respiratory motion between images; then all T1- and T2-prepared frames were aligned to the center frame, and T1 and T2 maps were generated from these motion-corrected images by fitting a mono-exponential decay curve at each pixel. The mid-ventricular short-axis and the 4-chamber images were manually contoured to outline the endocardium and epicardium, and the average myocardial T1 and T2 values were calculated for all patients. LGE measurement was

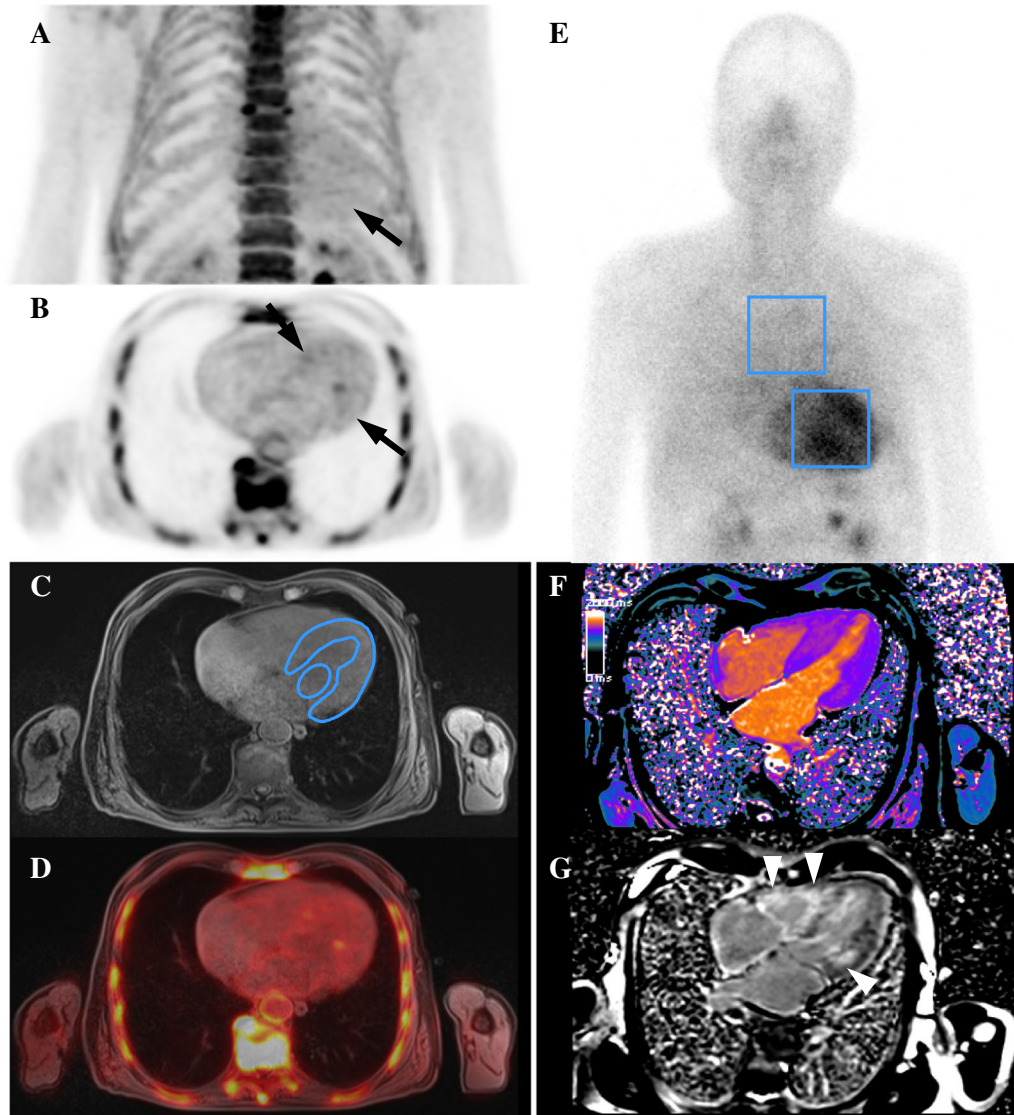


Figure 1. Example of a 81-year-old man with wt-TTR CA. Maximum intensity projection (A) shows faint ¹⁸F-NaF uptake over the myocardium (arrow). Axial PET (B), Dixon water MRI (C) and fusion (D) show a relatively homogeneous distribution of the radiotracer over the left myocardium (arrows). The M/B ratio is 1.13, while early-phase ^{99m}Tc-HMDP projection (E) shows much higher contrast with a H/M ratio calculated at 1.82. The average myocardial T1 calculated on the parametric map (F) is 1460 ms and PSIR image (G) shows diffuse late Gadolinium enhancement over the right and left myocardium with a QALE score of 14 (arrowheads).

evaluated on the short-axis PSIR sequence at the base, mid-ventricle, and apical portions; the Query Amyloid Late Enhancement (QALE) score was calculated at each level on a 5-point scale (0, absent; 1, non-specific or non-circumferential subendocardial; 2, circumferential subendocardial; 3, non-circumferential transmural; and 4, circumferential transmural), then summed for a maximum of 12 points, to which 6 points were added if right ventricle LGE was also present, as previously reported.^{10,13} Finally, the extracellular volume fraction was calculated with the following formula¹⁴:

$$\text{Extracellular volume (\%)} = (100 - \text{hematocrit}) \times \frac{\left(\frac{1}{T_{1\text{post-enhancement}}} - \frac{1}{T_{1\text{native}}} \right)_{\text{myocardium}}}{\left(\frac{1}{T_{1\text{post-enhancement}}} - \frac{1}{T_{1\text{native}}} \right)_{\text{blood pool}}}$$

Diagnosis of Cardiac Amyloidosis

All patients underwent a physical examination, electrocardiogram, transthoracic echocardiography, and standard

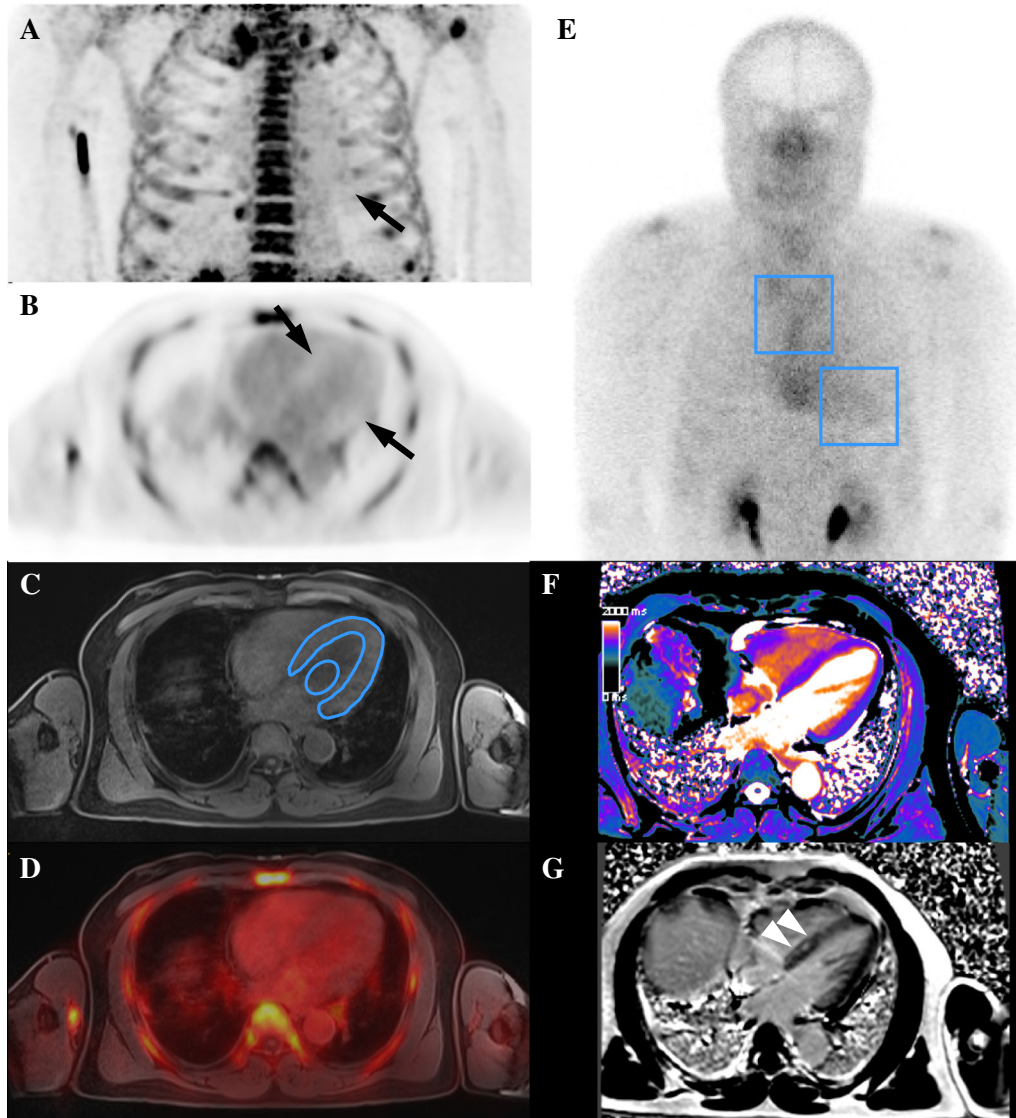


Figure 2. Example of a 68-year-old man with AL CA. Maximum intensity projection (A) shows absence of ¹⁸F-NaF uptake over the myocardium (arrow). Axial PET (B), Dixon water MRI (C) and fusion (D) show a net decrease of myocardial uptake compared to the neighboring blood pool (arrows). The M/B ratio is 0.72 and the H/M ratio calculated on early-phase ^{99m}Tc-HMDP projection (E) is 0.86. The average myocardial T1 calculated on the parametric map (F) is 1450 ms and PSIR image (G) shows late Gadolinium enhancement predominating over the septum with a QALE score of 10 (arrowheads).

biological tests (including serum assays of ultrasensitive cardiac troponin T, N-terminal pro-brain natriuretic peptide [NTproBNP], and creatinine). Diagnosis of CA was confirmed by endomyocardial biopsy or by the association of clinical, biological and imaging abnormalities, together with peripheral tissue biopsy. Pathologic specimens were interpreted after proper staining by Congo red, anti-TTR, anti- κ , and anti- λ antibodies, as previously described.⁶

Statistical Analysis

Statistical analyses were performed with MedCalc 12.2.1.0 (MedCalc Software bvba, Ostend, Belgium). Continuous variables were compared between patient groups using the Mann-Whitney test and categorical variables using the Fischer exact test. A *P* value < 0.05 indicated statistical significance.

Table 2. Population characteristics

	TTR (n = 16)	AL (n = 7)	No CA (n = 4)	P = *	P = **
Clinical					
Age, years	73 ± 9	69 ± 7	54 ± 18	0.05	0.06
Male	10 (63)	5 (71)	4 (100)	NS	NS
Hypertension	10 (63)	4 (57)	1 (25)	NS	NS
NHYA class III-IV	6 (38)	2 (29)	1 (25)	NS	NS
Carpal tunnel syndrome	12 (75)	1 (14)	1 (25)	0.006	NS
Neuropathy	8 (50)	2 (29)	0 (0)	NS	NS
ECG					
Microvoltage	5 (31)	5 (71)	1 (25)	NS	NS
PR duration (ms)	168 ± 23	179 ± 38	169 ± 60	NS	NS
QRS duration (ms)	115 ± 36	92 ± 13	108 ± 14	NS	NS
Atrial fibrillation	5 (31)	0 (0)	1 (25)	NS	NS
Echocardiography					
LVEF (%)	50 ± 14	54 ± 8	53 ± 9	NS	NS
IVST (mm)	15 ± 4	15 ± 2	12 ± 5	NS	NS
Global strain (%)	- 12 ± 5	- 10 ± 10	- 14 ± 4	NS	NS
Laboratory					
Creatinine (μmol/L)	115 ± 37	114 ± 42	104 ± 15	NS	NS
HS-Troponin T (IU/mL)	56 ± 28	59 ± 47	39 ± 54	NS	NS
NTproBNP (ng/L)	2486 ± 1668	2083 ± 3136	709 ± 820	0.03	0.07

Values are mean ± SD (Mann-Whitney test) or n (%) (Fischer test)

TTR, transthyretin; AL, light-chain; CA, cardiac amyloidosis; NYHA, New York Heart Association; ECG, electrocardiogram; LVEF, left ventricular ejection fraction; IVST, interventricular septal thickness; NTproBNP, N-terminal pro-brain natriuretic peptide

*TTR vs AL; **CA vs no-CA

RESULTS

Population Characteristics

Population characteristics are summarized in Table 2. TTR CA was diagnosed in 16 patients (7 wt-TTR, 9 m-TTR), AL CA in 7 patients and no-CA in 4 patients. There was a trend for older age in TTR than in AL CA patients. A carpal tunnel syndrome was significantly more frequent in TTR than in AL CA patients, and NTproBNP levels were significantly higher in TTR than in AL CA patients. The other clinical, electrocardiographic, echocardiographic, and biological parameters were not significantly different between patient groups.

PET Results

Visual interpretation of PET images revealed a relative increase in myocardial ¹⁸F-NaF uptake compared to neighboring blood pool in only 3 patients, all with TTR CA (3/16), and a relative decrease in myocardial uptake in 13 patients, including 7 with AL CA (7/7), 3 without CA (3/4), and 3 with TTR CA (3/16). Representative examples of a positive and a

negative PET patient are shown in Figures 1 and 2. The remaining patients had myocardial uptake similar to the blood pool. Using semi-quantification, M/B ratios (Table 3, Figure 3) were significantly higher in TTR CA patients (1.00 ± 0.12) than in AL CA patients (0.81 ± 0.06, *P* = 0.001) or in patients without CA (0.73 ± 0.16, *P* = 0.006). M/B ratios were also significantly higher in CA patients put together than in no-CA patients (*P* = 0.02, Table 3). Among TTR CA patients, M/B ratio was slightly higher in wt-TTR (1.01 ± 0.13) than in m-TTR patients (0.98 ± 0.12), although not significantly. The optimal ¹⁸F-NaF M/B cut-off by ROC analysis to distinguish TTR CA from AL CA was ≥ 0.90 (area under the ROC curve, AUC = 0.937; sensitivity 81.2%, specificity 100.0%). Classification of patients between TTR and AL using this cut-off reached significance with *P* = 0.0005. By comparison, classification of patients using ^{99m}Tc-HMDP H/M ratio with the previously published cut-off ≥ 1.21 reached higher significance with *P* < 0.0001 (Figure 3). The mean basal-to-apical ¹⁸F-NaF ratio among patients above the 0.90 cut-off averaged 1.45±0.43, indicating relative apical sparing of bone tracer uptake.

Table 3. Metabolic and functional parameters measured using ¹⁸F-NaF PET/MRI and early-phase diphosphonate imaging

	TTR (n = 16)	AL (n = 7)	No CA (n = 4)	P = *	P = **
¹⁸ F-NaF M/B ratio	1.00 ± 0.12	0.81 ± 0.06	0.73 ± 0.16	0.001	0.02
^{99m} Tc-HMDP H/M ratio	1.56 ± 0.28	1.01 ± 0.12	0.96 ± 0.18	0.0006	0.09
LVEF (%)	52 ± 16	61 ± 8	48 ± 7	NS	NS
Indexed EDV (mL/m ²)	78 ± 24	62 ± 18	96 ± 28	NS	NS
Indexed ESV (mL/m ²)	41 ± 21	24 ± 9	51 ± 21	0.03	NS
Septal thickening (mm)	16 ± 5	13 ± 4	13 ± 4	NS	NS
Myocardial mass (g/m ²)	110 ± 30	100 ± 31	104 ± 41	NS	NS
T1, ms	1410 ± 72	1406 ± 90	1278 ± 35	NS	0.004
T2, ms	43 ± 3	45 ± 4	45 ± 4	NS	NS
QALE score	10.75 ± 5.04	9.43 ± 6.16	3.50 ± 3.42	NS	0.03
Extracellular volume (%)	48 ± 11	43 ± 9	33 ± 8	NS	0.01
Pericardial effusion	6 (38)	1 (14)	2 (50)	NS	NS

Values are mean ± SD (Mann-Whitney test) or n (%) (Fischer test)

TTR, transthyretin; AL, light-chain; CA, cardiac amyloidosis; M/B, myocardial-to-blood pool; H/M, heart-to-mediastinum; LVEF, left ventricular ejection fraction; EDV, end-diastolic volume; ESV, end-systolic volume; QALE, query amyloid late enhancement

*TTR vs AL; **CA vs no-CA

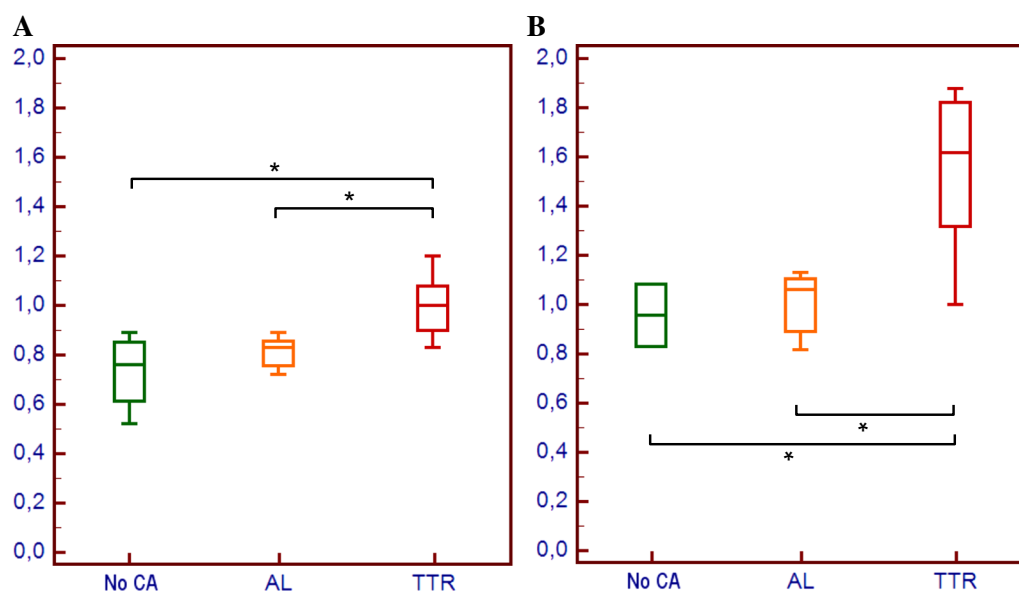


Figure 3. Box plots of ¹⁸F-NaF M/B ratios (A) and ^{99m}Tc-HMDP H/M ratios (B) show significant higher bone tracer uptake in TTR CA patients, compared with AL CA and no-CA patients (* < 0.05).

MRI Results

Among MRI parameters, the T1 was significantly longer in CA patients, compared with no-CA patients, 1409 ± 76 vs 1278 ± 35 ms, respectively ($P = 0.004$, Table 3). The optimal T1 cut-off by ROC analysis to distinguish CA from no-CA was ≥ 1315 ms (AUC =

0.962; sensitivity 91.3%, specificity 100.0%). Classification of patients between CA and no-CA using this cut-off reached significance with $P = 0.0009$. The LGE QALE score was also significantly higher in CA than in no-CA patients, 10.35 ± 5.30 vs 3.50 ± 3.42 , respectively ($P = 0.03$). The optimal QALE cut-off by ROC analysis to distinguish CA from no-CA was ≥ 5 (AUC =

0.848; sensitivity 82.6%. specificity 75.0%) and classification of patients using this cut-off reached significance with $P = 0.03$. Finally, the extracellular volume fraction was significantly higher in CA than in no-CA patients, 46 ± 10 vs 33 ± 8 % ($P = 0.01$). The optimal cut-off by ROC analysis to distinguish CA from no-CA was ≥ 32 % (AUC = 0.897; sensitivity 95.5%. specificity 75.0%) and classification of patients using this cut-off reached significance with $P = 0.005$. The other MRI parameters did not differ significantly between CA and no-CA patients, including LVEF, myocardial mass, and septal thickening. There was no significant difference in MRI parameters between TTR CA and AL CA patients, except for the left ventricle ESV, which appeared significantly lower in AL CA than in TTR CA, 24 ± 9 vs 41 ± 21 mL/m², respectively ($P = 0.03$, Table 3).

DISCUSSION

Our study shows that ¹⁸F-NaF PET is able to distinguish TTR from AL/no CA patients, with equivalent performance compared with ^{99m}Tc-HMDP, but only when M/B semi-quantification is used, as visual interpretation shows lower contrast. In addition, MRI can distinguish patients with CA from no-CA patient with a strong suspicion of CA, using the T1 mapping and LGE. Simultaneous PET/MRI imaging allows full cardiac assessment in a one-stop-shop setting.

The diagnostic value of ¹⁸F-NaF PET, based on the assumption that the type of amyloid protein affects local homeostasis of calcium, has been a matter of debate in the recent literature. Indeed, the first two case reports showed discrepant results.^{7,15} In the first one, the authors found moderate myocardial ¹⁸F-NaF uptake on PET/CT in a patient with mutant (Val122Ile) TTR CA, while PET/CT was negative in another patient with AL CA. To note, myocardial-to-background ratios showed a slow decrease between early (20 minutes post-injection) and delayed (1 hour post-injection) PET/CT images. In the second one, PET/CT did not show significant myocardial ¹⁸F-NaF uptake above background in two patients with TTR CA, one with an m-TTR (Ile68Leu) and one with a wt-TTR, on a 3-phase imaging (0, 15, and 60 minutes post-injection). However, no semi-quantification was provided; by reviewing the article figures, there is actually some ¹⁸F-NaF uptake, undistinguishable from the blood pool uptake, and therefore, we can assume that the M/B ratio would be around 1.00 in both patients, which is concordant with the mean M/B ratio found in the present study. In two recent series,^{8,9} including 7 CA patients each (5 TTR + 2 AL and 4 TTR + 3 AL, respectively), the authors confirmed the higher myocardial ¹⁸F-NaF uptake in TTR CA than in AL CA

patients. In the first series, conducted with PET/CT 1 h post-injection, the mean SUV over the entire myocardium was 58% higher in TTR CA than in AL CA patients, and slightly higher in wt-TTR than in m-TTR patients. To note, the degree of uptake varied according to myocardial segment. In the second series, conducted with PET/MRI using a dynamic acquisition over 90 minutes starting 5 minutes post-injection, myocardial target-to-background ratios after 1 h were 48% higher in TTR CA than in AL CA patients, with a patchy pattern of uptake. In our series, M/B ratio was only 24% higher despite we measured it within the same delay post-injection.

Cardiac MRI has been a reference tool for the diagnosis and functional evaluation of cardiac amyloidosis over the last decade, as reported in many publications.^{16–18} In our study, all patients underwent extensive cardiac MRI, including parametric imaging and semi-quantitative evaluation of late gadolinium enhancement. In line with previous reports, we found a significant increase of native myocardial T1 and extracellular volume fraction in patients with CA compared to those without CA, secondary to amyloid protein deposits in myocardial tissue. Several authors have also reported different MRI characteristics between TTR and AL CA patients, with a trend for higher QALE score in the former than in the latter,¹¹ whereas native myocardial T1 was longer in AL than in TTR CA patients, probably because of myocardial edema.¹⁰ Unfortunately, we did not find such differences in our study.

Although semi-quantification of ¹⁸F-NaF uptake can reliably distinguish TTR CA from AL CA in our series, visual interpretation was much more challenging. Indeed, a higher myocardial uptake compared to background was seen in only 3/16 patients with TTR CA (the remaining patients having a myocardial uptake equivalent or slightly lower to the blood pool), while a relative decrease in myocardial uptake was observed in all (7/7) patients with AL CA. Contrast is then very different from what is observed with ^{99m}Tc-labeled diphosphate imaging. Our study allows direct comparison between ¹⁸F-NaF and ^{99m}Tc-HMDP uptake in 24/27 patients: all TTR CA patients were strongly positive while all AL CA patients were negative on visual interpretation, without help of semi-quantification. Therefore, in view of performing PET/MRI one-stop-shop imaging, other ¹⁸F-labeled tracers should probably be preferred, such as markers of the amyloid plaque. Park et al. studied the specific binding of ¹⁸F-florbetapir to human myocardial AL and TTR amyloid deposits in 20 CA patients (10 TTR + 10 AL) and 10 non-amyloid controls on autopsy myocardial specimen by autoradiography.¹⁹ They demonstrated higher uptake of the radiotracer in AL CA patients than in TTR CA and

controls. These findings were later confirmed in vivo by Law et al. using ¹⁸F-florbetaben PET/CT and measurement of the retention index in 10 CA patients (5 TTR + 5 AL) and 4 hypertensive controls.²⁰ In addition, Wagner et al. showed the very high specificity of ¹⁸F-florbetapir for cardiac and extracardiac amyloid involvements in 17 CA patients (2 TTR + 15 AL) and suggested that this tracer may become the main tracer for the diagnosis of systemic amyloidosis in the future.²¹ Finally, the recent pilot study from Dietemann et al. in 9 patients (1 AL + 8 TTR) has shown high tumor-to-background ratios in CA patients compared to no-CA patients (n = 3) using ¹⁸F-flutemetamol, 1.46 vs 1.06, respectively (*P* = 0.03).²²

Our study has some limitations. Despite a relatively large cohort of patients with CA (n = 23), the number of patients with non-amyloid cardiopathies is limited (n = 4), which makes it difficult to compare metabolic, morphological and functional parameters between CA and non-CA patients. Segmental assessment of ¹⁸F-NaF distribution within the myocardium was not possible because the contrast was too low to build polar maps; however, by simply drawing circular ROIs above a basal segment and the apex, we found a mean basal-to-apical ratio of 1.45 ± 0.43, indicating relative apical sparing of bone tracer uptake, as previously described using ^{99m}Tc-HMDP.²³ There is also a recruitment bias as many candidates for ¹⁸F-NaF imaging (approximately 30% of patients in our experience) could not undergo MRI at 3 T due to the presence of a pacemaker or other metallic devices, which are not contra-indicated when using PET/CT. However, this technique could be useful for a one-stop-shop evaluation of bone tracer uptake, tissue characterization, and cardiac function in patients needing rapid diagnostic work-up.

CONCLUSION

¹⁸F-NaF PET/MRI shows comparable diagnostic performance as ^{99m}Tc-HMDP when M/B semi-quantification is used. However, contrast is much lower, and visual interpretation may not be able to distinguish TTR from AL/no CA in routine with enough reliability. This technique could be useful for a one-stop-shop evaluation of bone tracer uptake, tissue characterization, and cardiac function in patients needing rapid diagnostic work-up.

NEW KNOWLEDGE GAINED

¹⁸F-NaF PET is able to distinguish patients with TTR cardiac amyloidosis from those with AL or without cardiac amyloidosis

Visual analysis of ¹⁸F-NaF uptake is challenging because of low contrast between myocardium and blood pool but semi-quantification demonstrates good performances

MRI with T1 mapping, late gadolinium enhancement, and calculation of the extracellular volume is able to distinguish patients with cardiac amyloidosis from those without cardiac amyloidosis

Simultaneous assessment of PET and MRI may be useful for a one-stop-shop evaluation of bone tracer uptake, tissue characterization, and cardiac function in patients needing rapid diagnosis

Disclosures

All authors have approved the manuscript, and agree with its submission to the Journal of Nuclear Cardiology. There is no financial or other relation that could lead to a conflict of interest.

Ethical approval

The procedure followed was in accordance with the ethical standards guidelines of the responsible committee on human experimentation.

References

1. Merlini G, Bellotti V. Molecular mechanisms of amyloidosis. *N Engl J Med* 2003;349:583-96.
2. Mohty D, Damy T, Cosnay P, Echahidi N, Casset-Senon D, Viot P, et al. Cardiac amyloidosis: updates in diagnosis and management. *Arch Cardiovasc Dis* 2013;106:528-40.
3. Holzmann M, Nicko A, Kuhl U, Noutsias M, Poller W, Hoffmann W, et al. Complication rate of right ventricular endomyocardial biopsy via the femoral approach: A retrospective and prospective study analyzing 3048 diagnostic procedures over an 11-year period. *Circulation* 2008;118:1722-8.
4. Gillmore JD, Maurer MS, Falk RH, Merlini G, Damy T, Dispenzieri A, et al. Nonbiopsy diagnosis of cardiac transthyretin amyloidosis. *Circulation* 2016;133:2404-12.
5. Deux JF, Damy T, Rahmouni A, Mayer J, Plante-Bordeneuve V. Noninvasive detection of cardiac involvement in patients with hereditary transthyretin associated amyloidosis using cardiac magnetic resonance imaging: A prospective study. *Amyloid* 2014;21:246-55.
6. Galat A, Rosso J, Guellich A, Van Der Gucht A, Rappeneau S, Bodez D, et al. Usefulness of (99m)Tc-HMDP scintigraphy for the etiologic diagnosis and prognosis of cardiac amyloidosis. *Amyloid* 2015;22:210-20.
7. Van Der Gucht A, Galat A, Rosso J, Guellich A, Garot J, Bodez D, et al. [¹⁸F]-NaF PET/CT imaging in cardiac amyloidosis. *J Nucl Cardiol* 2016;23:846-9.
8. Morgenstern R, Yeh R, Castano A, Maurer MS, Bokhari S. (18)Fluorine sodium fluoride positron emission tomography, a potential biomarker of transthyretin cardiac amyloidosis. *J Nucl Cardiol* 2017;25:1559-67.

9. Trivieri MG, Dweck MR, Abgral R, Robson PM, Karakatsanis NA, Lala A, et al. (18)F-sodium fluoride PET/MR for the assessment of cardiac amyloidosis. *J Am Coll Cardiol* 2016;68:2712-4.
10. Ridouani F, Damy T, Tacher V, Derbel H, Legou F, Sifaoui I, et al. Myocardial native T2 measurement to differentiate light-chain and transthyretin cardiac amyloidosis and assess prognosis. *J Cardiovasc Magn Reson* 2018;20:58.
11. Dzung JN, Valencia O, Pinney JH, Gibbs SD, Rowczenio D, Gilbertson JA, et al. CMR-based differentiation of AL and ATTR cardiac amyloidosis. *JACC Cardiovasc Imaging* 2014;7:133-42.
12. Galat A, Van der Gucht A, Guellich A, Bodez D, Cottureau AS, Guendouz S, et al. Early phase 99Tc-HMDP scintigraphy for the diagnosis and typing of cardiac amyloidosis. *JACC Cardiovasc Imaging* 2017;10:601-3.
13. Wan K, Sun J, Han Y, Liu H, Yang D, Li W, et al. Increased prognostic value of query amyloid late enhancement score in light-chain cardiac amyloidosis. *Circ J* 2018;82:739-46.
14. Messroghli DR, Moon JC, Ferreira VM, Grosse-Wortmann L, He T, Kellman P, et al. Clinical recommendations for cardiovascular magnetic resonance mapping of T1, T2, T2* and extracellular volume: A consensus statement by the Society for Cardiovascular Magnetic Resonance (SCMR) endorsed by the European Association for Cardiovascular Imaging (EACVI). *J Cardiovasc Magn Reson* 2017;19:75.
15. Gagliardi C, Tabacchi E, Bonfiglioli R, Diodato S, Nanni C, Guidalotti P, et al. Does the etiology of cardiac amyloidosis determine the myocardial uptake of [18F]-NaF PET/CT? *J Nucl Cardiol* 2016;24:746-9.
16. Maceira AM, Prasad SK, Hawkins PN, Roughton M, Pennell DJ. Cardiovascular magnetic resonance and prognosis in cardiac amyloidosis. *J Cardiovasc Magn Reson* 2008;10:54.
17. Karamitsos TD, Piechnik SK, Banypersad SM, Fontana M, Ntusi NB, Ferreira VM, et al. Noncontrast T1 mapping for the diagnosis of cardiac amyloidosis. *JACC Cardiovasc Imaging* 2013;6:488-97.
18. Fontana M, Chung R, Hawkins PN, Moon JC. Cardiovascular magnetic resonance for amyloidosis. *Heart Fail Rev* 2015;20:133-44.
19. Park MA, Padera RF, Belanger A, Dubey S, Hwang DH, Veeranna V, et al. 18F-florbetapir binds specifically to myocardial light chain and transthyretin amyloid deposits: Autoradiography study. *Circ Cardiovasc Imaging* 2015;8:e002954.
20. Law WP, Wang WY, Moore PT, Mollee PN, Ng AC. Cardiac amyloid imaging with 18F-florbetaben PET: A pilot study. *J Nucl Med* 2016;57:1733-9.
21. Wagner T, Page J, Burniston M, Skillen A, Ross JC, Manwani R, et al. Extracardiac (18)F-florbetapir imaging in patients with systemic amyloidosis: More than hearts and minds. *Eur J Nucl Med Mol Imaging* 2018;45:1129-38.
22. Dietemann S, Nkoulou R. Amyloid PET imaging in cardiac amyloidosis: A pilot study using (18)F-flutemetamol positron emission tomography. *Ann Nucl Med* 2019;33(8):624-8.
23. Van Der Gucht A, Cottureau AS, Abulizi M, Guellich A, Blanc-Durand P, Israel JM, et al. Apical sparing pattern of left ventricular myocardial (99m)Tc-HMDP uptake in patients with transthyretin cardiac amyloidosis. *J Nucl Cardiol* 2018;25:2072-9.

Publisher's Note Springer Nature remains neutral with regard to jurisdictional claims in published maps and institutional affiliations.